2005:3

Subspace Analysis of Indoor UWB Channels

Aawatif Menouni Hayar

Mobile Communications Laboratory, Institut Eurécom, 06904 Sophia Antipolis Cedex, France
Email: menouni@eurecom.fr

Raymond Knopp

Mobile Communications Laboratory, Institut Eurécom, 06904 Sophia Antipolis Cedex, France
Email: knopp@eurecom.fr

Rachid Saadane

UFR SysCom2, Faculté des Sciences, Université Mohammed V-Agdal, Rabat, Morocco
Email: saadane@eurecom.fr

This work aims at characterizing the second-order statistics of indoor ultra-wideband (UWB) channels using channel sounding techniques. We present measurement results for different scenarios conducted in a laboratory setting at Institut Eurécom. These are based on an eigendecomposition of the channel autocovariance matrix, which allows for the analysis of the growth in the number of significant degrees of freedom of the channel process as a function of the signaling bandwidth as well as the statistical correlation between different propagation paths. We show empirical eigenvalue distributions as a function of the signal bandwidth for both line-of-sight and non-line-of-sight situations. Furthermore, we give examples where paths from different propagation clusters (possibly arising from reflection or diffraction) show strong statistical dependence.

Keywords and phrases: indoor UWB channel measurements, subspace analysis, number of degrees of freedom.

1. INTRODUCTION

The use of ultra-wideband (UWB) signaling techniques are being considered for short-range indoor communications, primarily for next-generation high-bit-rate *wireless personal area networks (WPANs)*. Initial work in this direction was carried out by Scholtz [1, 2], using the most common form of signaling based on short-term impulses, where information is carried in their position. Such techniques, as well as others, are being considered in the standardization process of the IEEE 802.15.3a WPAN proposal (see http://grouper.ieee.org). At the same time, regulatory aspects are quickly being defined by the FCC.

The expected bandwidths of these systems are of the order of one GHz, which has significant implications both for systems design and implementation. The goal of this work is to determine the result of these extremely large system bandwidths on the second-order statistics of the propagation channel as it is seen by the underlying system. We are primarily interested in assessing the growth in degrees of freedom (DoFs) needed to characterize the channel as a function of the system bandwidth.

Other measurements studies on the UWB propagation channel are appearing in [3, 4, 5, 6] for instance. This work is complementary in the sense that we use a state-of-the-art wideband measurement equipment to determine the growth of the number of significant *free DoF*s of the propagation channel as a function of the signaling bandwidth, based on subspace techniques. The number of significant DoF is related both to the number of resolvable multipath components and to the diversity order or richness of the indoor channel. Measurements are carried out for both line-of-sight (LOS) and non-line-of-sight (NLOS) short-range indoor communications.

Section 2 describes the measurement equipment used in this study as well as the propagation environment. In Section 3, we outline the subspace methods used for analyzing the second-order statistics of the propagation channel. Section 4 describes the numerical results and Section 5 presents the conclusions of this study.

2. UWB CHANNEL MEASUREMENT SCENARIO

2.1. Equipment and measurement setup

The measurement device used in this study is a wideband vector network analyzer (VNA) which allows complex transfer function (e.g., S_{21}) parameter measurements in the
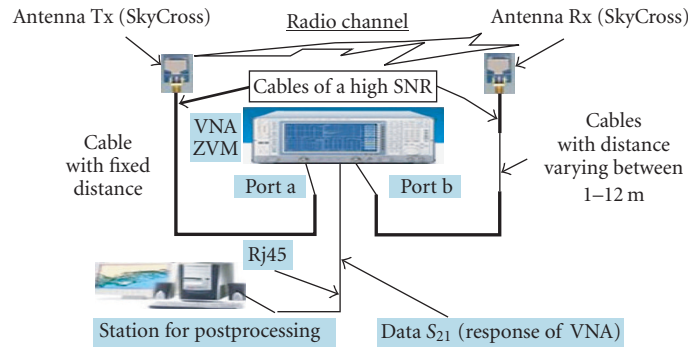
FIGURE 1: Channel measurement setup.

frequency domain extending from 10 MHz to 20 GHz. This instrument has low inherent noise (less than -110 dBm for a measurement bandwidth of 10 Hz) and high measurement speed (less than 0.5 ms/point). The maximum number of equally spaced frequency samples (amplitude and phase) per measurement is 2001. The measurement data are acquired and controlled remotely using the RSIB protocol over an Ethernet network permitting offline signal processing and instrument control in Matlab. The measurement system is shown in Figure 1. In order to perform truly wideband measurements with sufficient resolution, several bands can be concatenated using consecutive measurements. In this study, we performed measurements from 3 to 9 GHz by concatenating 3 groups of 2001 frequency samples per 2 GHz subband (3–5 GHz, 5–7 GHz, and 7–9 GHz). This yields a 1 MHz spacing between frequency samples. As discussed in the following section, this resolution was found to be sufficient for the analysis of the second-order statistics of the channel impulse response (CIR). The corresponding maximum time-domain resolution is $T = 167$ picoseconds in a 1 microsecond time interval. The use of passive elements in the measurement apparatus (cables, SMA connectors, etc.) imposed a systematic and frequent calibration measurement (which was controlled remotely), in order to compensate undesirable frequency-dependent attenuation factors that could affect the collected data. Following the VNA's manual recommendations, the calibration "through response" type was selected, and the cables and the connectors were included in this calibration.

The wideband antennas employed in this study are omnidirectional in the vertical plane and have an approximate bandwidth of 7.5 GHz (varying from 3.1 to 10 GHz). They are not perfectly matched across the entire band, with a VSWR (voltage standing-wave ratio, VSWR $= (1 + |\rho|)/(1 - |\rho|)$, ρ is the wave's coefficient of reflection) varying from 2 to 5 (e.g., the antenna has an efficiency of about 82% at 5.2 GHz; see www.skycross.com). The frequency response of the antenna is shown in Figure 2, where we see that it is not completely flat over the band of interest. In what follows, the antennas are considered to be part of the channel response. This is of practical interest, since the true response to the antenna depends heavily on its immediate vicinity, especially in
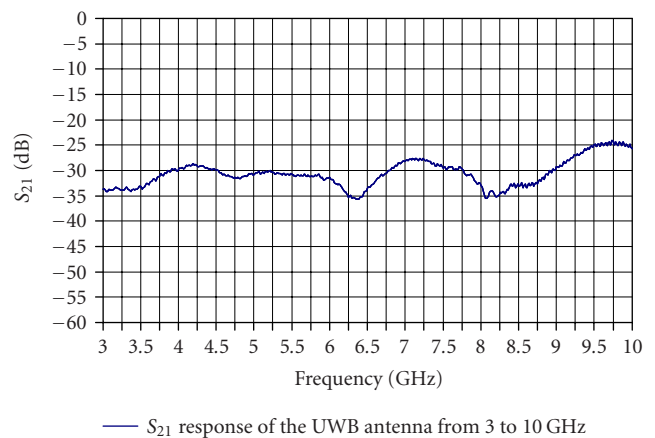
FIGURE 2: S_{21} response for the SkyCross UWB antenna.

the type of applications envisaged for UWB systems, namely, low-height and peer-to-peer communications with the presence of nearby obstacles (people, furniture, walls, etc.). As a result, the true response of the antenna is of secondary importance from a system's point of view.

2.2. Measurement environment

Measurements are performed at spatially different locations for both LOS and NLOS. The experiment area is set by fixing the transmitting antenna on a mast at 1 m above the ground on a horizontal linear grid (20 cm) close to VNA and moving the receiver antenna to different locations on a horizontal linear grid (50 cm) in 1 cm steps. In this configuration, we assure that the attenuation due to short-term fading effects is virtually constant for all combinations of transmitter and receiver positions. This is explained in more detail in the following section. The transmitter/receiver positioning is depicted in Figure 3. The height of receiver antenna was also 1 m above the ground. This type of propagation scenario clearly targets peer-to-peer applications.

A measurement scenario is described by the transmitter/receiver separation and the presence or lack of a LOS component. The latter was achieved by inserting a large
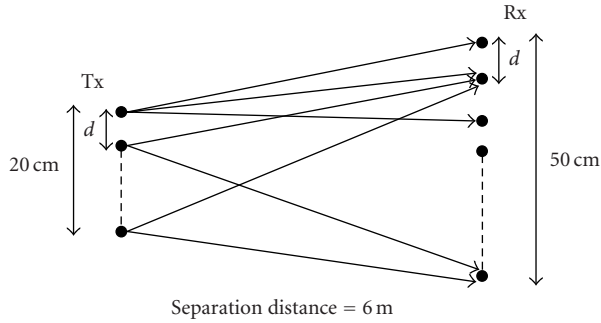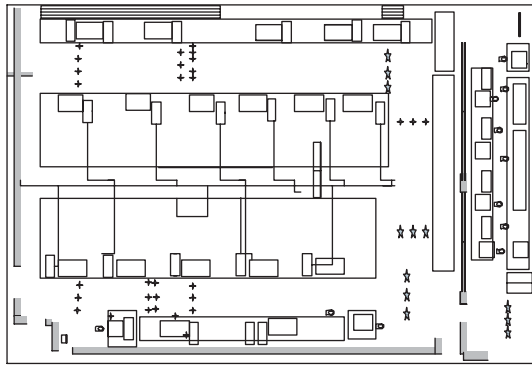
FIGURE 3: Transmitter/receiver positioning.

+ Rx antenna
☆ Tx antenna

FIGURE 4: Channel measurement environment.

obstacle between the transmitter and the receiver in order to block the LOS path. Because of the proximity of the transmitter and the receiver, this also has the effect of reducing the amount of scattered paths which reach the receiver and thus reducing the richness of the propagation channel. For the two measurement scenarios with transmitter/receiver separation of 6 m representing NLOS and LOS communications, we acquired 1000 different complex frequency responses each. All numerical results reported in this paper refer to the two 6 m scenarios. Similar experiments with fewer measurements were also made for transmitter/receiver separations varying from 1 to 12 m in both LOS and NLOS configurations. The measurements were carried out in Institut Eurécom's Mobile Communication Laboratory, which is a typical laboratory environment (radio-frequency equipment, computers, tables, chairs, metallic cupboard, glass windows, etc.), as shown in Figure 4, rich in reflective and diffractive objects.

3. UWB EIGENANALYSIS

The classical approach [7, 8, 9] used for the characterization of the selectivity of multipath fading channels is based on root mean square (RMS) delay spread T_d. This parameter or

equivalently the *coherence bandwidth* B_c defined as

$$B_c = \frac{k}{T_d}, \tag{1}$$

where $0 < k < 1$ is a constant, is widely used as a measure of the channel's frequency selectivity. This approach is generally correct when the signal bandwidth comprises a small number of coherence bandwidths. But in wideband or UWB channels, this study will show that the coherence bandwidth can only be seen as a local measure and does not give an accurate description of channel selectivity. Similar ideas for channel bandwidths on the order of tens of megahertz were also suggested in [10].

3.1. Eigendecomposition of covariance matrix

The radio-propagation channel is randomly time varying due to variations in the environment and the mobility of transmitters and receivers. It is classically represented, following the work of Bello [11, 12], by its input delay-spread function $h(t, \tau)$ called also, by abuse of language, the time-varying CIR. The variable t in the CIR notation represents the time-varying behavior of the channel caused by the mobility of either the transmitter, the receiver, or the scatterers. The second variable τ represents the delay domain in which we characterize the channel regarding the most important arriving paths. We consider for each measurement a fixed position at the transmitter and the receiver sides, and a static environment (at least during the time frame of one measurement). We are thus considering a static channel and we can then simplify the notation of the CIR by dropping its dependence on t. In what follows, $h(\tau)$ is simply replaced by $h(t)$. Let $\mathbf{h}(t) = [h_{W,1}(t), h_{W,2}(t), \ldots, h_{W,N}(t)]$ be the channel process obtained from measurements for N different antenna configurations, where $h_{W,i}(t)$ is expressed as

$$h_i(t) = g_i(t) + n_i(t), \quad i = 1, \ldots, N, \tag{2}$$

where $n_i(t)$ is a zero-mean additive white Gaussian noise with power spectral density equal to σ_n^2 at all frequencies in the bandwidth of interest. We neglect any nonlinear perturbation caused by measurement elements (e.g., VNA amplifiers), which were treated in a more general setting in [13]. We include the frequency response of the antenna as part of the channel response as argued in the previous section, and moreover, the linear response of the equipment is assumed to be perfectly accounted for in the calibration of the measurement apparatus. The noise process, resulting from thermal noise in the receive chain of the VNA and the noise generated by the device itself, is assumed to be white in the band of interest. We therefore have that $\mathbf{g}(t) = [g_1(t), g_2(t), \ldots, g_N(t)]$ are the observations of the noise-free channel process corresponding to N observation positions. Due to the rapid variation of the wave's phase (from 0 to 2π over one wavelength), we can assume that the received electric field at each position represents a zero-mean process, and thus $g(t)$ is taken to be zero mean. We remark that this does not rule out the possibility of LOS propagation as will be treated shortly.
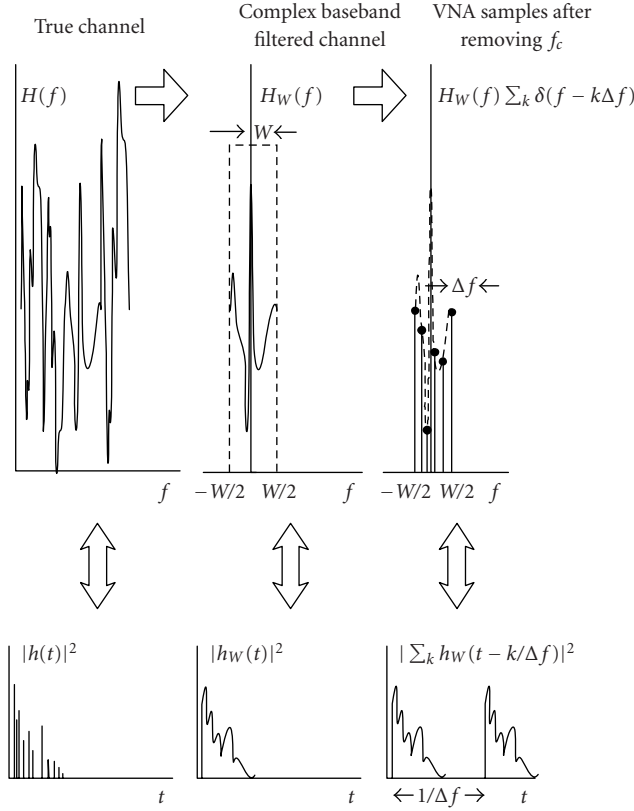
FIGURE 5: Channel representations.

The VNA provides samples of the observed channel process in the frequency domain, $H(k\Delta f)$, where Δf is the frequency separation, in our case 1 MHz. Furthermore, it is a filtered version of the channel response, where the filter corresponds to an ideal bandpass filter of bandwidth W centered at $f_c = (f_{\max} - f_{\min})/2$, as shown in Figure 5. After removing the carrier frequency f_c, we denote the complex baseband equivalent filtered channel by $h_W(t)$. By sampling the frequency response in the VNA and removing the carrier frequency, we obtain an aliased version of $h_W(t)$ denoted by $\tilde{h}_W(t) = \sum_k h_W(t - k/\Delta f)$. The time-domain samples obtained by performing an inverse discrete Fourier transform (IDFT) on the vector $\mathbf{H} = (H(0) \ H(\Delta f) \ \cdots \ H((N-1)\Delta f))^{\mathrm{T}}$ are samples of $\tilde{h}_W(t)$ at sampling frequency W Hz. We note that the choice of frequency separation Δf has an impact on how closely $\tilde{h}_W(t)$ approximates $h_W(t)$ in the interval $[0, 1/\Delta f)$. In our case, the choice of $\Delta f = 1$ MHz guarantees that the approximation will be very accurate since the typical delay spread of the considered channels is less than 100 nanoseconds and therefore time-domain aliasing will not distort the channel measurement. For this reason, we assume in what follows that the measurement equipment provides perfect samples of $h_W(t)$.

Our approach to characterize the UWB propagation channel is based on the analysis of the channel subspace and the eigendecomposition of the covariance matrix, $\mathbf{K_h}$, of the samples of $h_W(t)$, denoted by the vector $\mathbf{h} =$

$(h_W(0) \ h_W(1/W) \ \cdots \ h_W((p-1)/W))^{\mathrm{T}}$, where p is the length of the channel used for statistical analysis with $0 \le p \le 1/\Delta F - 1/W$. This allows us to estimate the number of DoF characterizing $h_W(t)$ [14]. A similar approach for estimating the (finite) unknown number of Gaussian signals using a finite set of noisy observations is described in [15, 16]. These techniques amount to determining the finite dimension of the signal subspace.

In order to estimate the true covariance matrix $\mathbf{K_h}$, we use statistical averages based on observations from (20×50) positions. The sample covariance matrix is a maximum-likelihood estimate, under the assumption of a large number of independent channel observations [17] which arise from the different transmitting and receiving antenna positions as explained earlier. The separation between positions on the grids must be large enough to obtain sufficient variation of the wave's phase, $\Delta\phi^1$, in order to extract all the DoF of the channel. On the other hand, the separation must be small enough to ensure that the distance between transmitter and the receiver (6 m in our primary measurement scenario) remains virtually constant. If both constraints are satisfied, we can assume that $\mathbf{K_h}$ will depend solely on the slowly varying parameters (distance, arrival angles, scatterers, geometrical settings, etc.) and thus will not vary significantly across the set of the total transmitter and receiver positions. The covariance matrix of measured channel samples, $\mathbf{h}$, is written as

$$\mathbf{K_h} = E[\mathbf{hh}^{\mathrm{H}}] = E[\mathbf{gg}^{\mathrm{H}}] + \sigma_n^2 \mathbf{I}, \qquad (3)$$

where $\mathbf{g}$ is a vector of samples of the noise-free channel process, and $\mathbf{I}$ is the identity matrix. The maximum-likelihood covariance matrix estimate computed from N statistically independent channel observation with length p and $p < N$ is given by [17]

$$\mathbf{K_g}^N = \mathbf{K_h}^N = \frac{1}{N} \sum_{i=1}^{N} \mathbf{h}_i \mathbf{h}_i^{\mathrm{H}}. \qquad (4)$$

The assumption of $p < N$ holds in our case since we ensure that the length of sampled CIR is less than 1000 samples, which represents the total number of channel observations for one scenario. For small d/λ, the assumption of independent observations and thus that the channel samples are spatially decorrelated is justified in an indoor MIMO setting in [18]. In the context of our measurements, the multiple transmitter/receiver grid can equivalently be seen as a large (50×20) MIMO system.

The covariance matrix is Hermitian and positive definite. For this reason, a unitary matrix $\mathbf{U_h}$ exists such that the Karhunen-Loève (KL) expansion gives

$$\mathbf{K_h}^N = \mathbf{U_h} \Lambda_\mathbf{h} \mathbf{U_h}^{\mathrm{H}} = \sum_{i=1}^{N} \lambda_i(\mathbf{h}) \psi_i(\mathbf{h}) \psi_i^{\mathrm{H}}(\mathbf{h}), \quad \mathbf{U_h}^{\mathrm{H}} \mathbf{U_h} = \mathbf{I}_N, \quad (5)$$

---

[1] $\Delta\phi = 2\pi d/\lambda$ is the wave's phase variation between two positions, d is the corresponding distance, and λ is the wavelength varying from 3 to 10 cm for a UWB channel bandwidth ranging from 3 to 10 GHz.

where $\lambda_1(\mathbf{h}) \geq \lambda_2(\mathbf{h}) \geq \cdots \geq \lambda_N(\mathbf{h})$, $\psi_i(\mathbf{h})$ is the ith column of $\mathbf{U_h}$, and $\mathbf{I}_N$ is the $N \times N$ identity matrix with N number of samples. $\lambda_i(\mathbf{h})$ and $\psi_i(\mathbf{h})$ are the ith eigenvalues and eigenvectors of $\mathbf{K_h}^N$, respectively. Decomposing (3) into principal and noise components yields

$$
\begin{aligned}
\mathbf{U}_{s,\mathbf{h}} &= [\psi_1(\mathbf{h}), \psi_2(\mathbf{h}), \dots, \psi_P(\mathbf{h})], \\
\lambda_1(\mathbf{h}) &\geq \lambda_2(\mathbf{h}) \geq \cdots \geq \lambda_L(\mathbf{h}), \\
\mathbf{U}_{n,\mathbf{h}} &= [\psi_{L+1}(\mathbf{h}), \psi_{L+2}(\mathbf{h}), \dots, \psi_N(\mathbf{h})], \\
\lambda_{L+1}(\mathbf{h}) &\geq \lambda_{L+2}(\mathbf{h}) \geq \cdots \geq \lambda_N(\mathbf{h}),
\end{aligned}
\tag{6}
$$

where $\mathbf{U}_{s,\mathbf{h}} \perp \mathbf{U}_{n,\mathbf{h}}$. $\mathbf{U}_{s,\mathbf{h}}$ defines the subspace containing both signal and noise components, whereas $\mathbf{U}_{n,\mathbf{h}}$ defines the noise-only subspace. L is the number of significant eigenvalues which also represents the channel DoFs [15], in the sense that any set of observations can be characterized by a set of approximately L independent random variables which excite L modes (their corresponding eigenvectors). In our case, the eigenvectors correspond to the samples of the eigenfunctions characterizing the propagation environment. They convey information regarding the statistical correlation between paths arriving at different time instants, since if in a particular eigenvector, ψ_i, we find several significantly spaced high-energy samples (paths), the same random variable with variance $\lambda_i(\mathbf{h})$ excites these samples and thus they exhibit statistical correlation.

3.2. Characterization of the total received energy

Following the eigendecomposition, we can define the normalized total received energy in an observation as $X = \mathbf{h}^{\mathrm{H}}\mathbf{h}/\overline{\mathbf{h}^{\mathrm{H}}\mathbf{h}}$, where the average channel energy is denoted by $\overline{\mathbf{h}^{\mathrm{H}}\mathbf{h}}$. We must distinguish two important cases, namely, the presence or lack of a LOS path in the received wave front. In general, we may express the filtered impulse response of the channel, assuming a discrete set of scatterers, as

$$
\begin{aligned}
h_W(t) &= A_0 e^{j\phi_0} \operatorname{sinc}(W(t - t_0)) \\
&\quad + \sum_{i>0} A_i e^{j\phi_i} \operatorname{sinc}(W(t - t_i)),
\end{aligned}
\tag{7}
$$

where A_0 represents the strength of the LOS component, $A_{i>0}$ the random amplitudes of scattered components, and t_i are the delays of each component. For a particular channel sample, we obtain

$$
\begin{aligned}
h(n) &= A_0 e^{j\phi_0} \operatorname{sinc}\left(W\left(\frac{n}{W - t_0}\right)\right) \\
&\quad + \sum_{i>0} A_i e^{j\phi_i} \operatorname{sinc}\left(W\left(\frac{n}{W - t_i}\right)\right).
\end{aligned}
\tag{8}
$$

In the characterization of the energy of the channel, $\mathbf{h}^{\mathrm{H}}\mathbf{h}$, the phase offset of the direct path can clearly be neglected, and thus we can assume that ϕ_0 is zero, even if it is truly a random quantity. Moreover, for a dense multipath environment, each $h(n)$ can be approximated by a Gaussian random variable with mean $A_0 \operatorname{sinc}(W(n/W - t_0))$ as is classically assumed

[19]. We can thus express the channel-energy moment generating function as

$$
G_X(s) = E[e^{sx}] = \int_{-\infty}^{+\infty} e^{sx} f_X(x) dx = L(f_X(x))\big|_{s=-s},
\tag{9}
$$

where L is the Laplace transform operator and $f_X(x)$ is the probability density function (pdf) of variable X. We can see from the last equation that $G_X(s)$ and $f_X(x)$ are Laplace transform pairs with $s = -s$. $G_X(s)$ can also be expressed as follows using the covariance matrix $\mathbf{K_h}$:

$$
G_X(s) = \frac{e^{\mathbf{m}^{\mathrm{H}}(\mathbf{I} - s\mathbf{K_h})^{-1}\mathbf{m}}}{\det(\mathbf{I} - s\mathbf{K_h})},
\tag{10}
$$

where the vector $\mathbf{m}$ has components $m(n) = A_0 \operatorname{sinc}(W(n/W - t_0))$ [20]. We will assume that $\mathbf{K_h}$ is characterized by L significant eigenvalues, $\lambda_i(\mathbf{h}) : i = 1, \dots, L$, which are positive. Furthermore, we constrain our treatment of the channel energy to the NLOS case since no attempt was made to estimate the LOS component strength, A_0, from our collected data. It is easily shown using the initial value theorem [21] that the pdf of the normalized channel energy can be approximated around the origin as

$$
\begin{aligned}
f_X(x) &\approx \frac{x^{(L-1)}}{(L-1)!} \frac{1}{\det(\mathbf{K_h})} \\
&= \frac{x^{(L-1)}}{(L-1)!} \frac{1}{\prod_i \lambda_i(\mathbf{h})} \quad \text{for } 0 \leq x \ll \min(\lambda_i(\mathbf{h})).
\end{aligned}
\tag{11}
$$

This indicates that around the origin, X behaves as an Erlang-L variable[2] with parameter $2\sigma^2 = \sqrt[L]{\prod_i \lambda_i(\mathbf{h})}$. The approximate cumulative distribution function can be expressed in terms of the incomplete Gamma function, or in terms of the Marcum-Q function, $Q_L(0, x)$, as

$$
\begin{aligned}
F_X(x) &= \gamma\left(\frac{x}{2\sigma^2}, L\right) = 1 - Q_L\left(0, \frac{\sqrt{x}}{\sigma}\right) \\
&\approx \frac{1}{\Gamma(L+1)}\left(\frac{x}{2\sigma^2}\right)^L \quad (0 \leq x \leq \prod_i \lambda_i(\mathbf{h})) \\
&= \frac{x^L}{\Gamma(L+1)\prod_i \lambda_i(\mathbf{h})}.
\end{aligned}
\tag{12}
$$

The above approximations can be found in [22]. Since the approximation is valid for small X, we are characterizing the region of the CDF in its left-hand tail. From the above expression, we see that we can use the slope of $\log(\text{CDF})$ to gain insight regarding the number of significant DoF for a particular average channel strength. This can also be seen equivalently as determining the inherent diversity order of the channel [23].

---

[2]The Erlang-L pdf of variable X is given by $f_X(x) = (x^{L-1}/(2\sigma^2)^L\Gamma(L))e^{-x/2\sigma^2}$, $x > 0$ and L an integer.
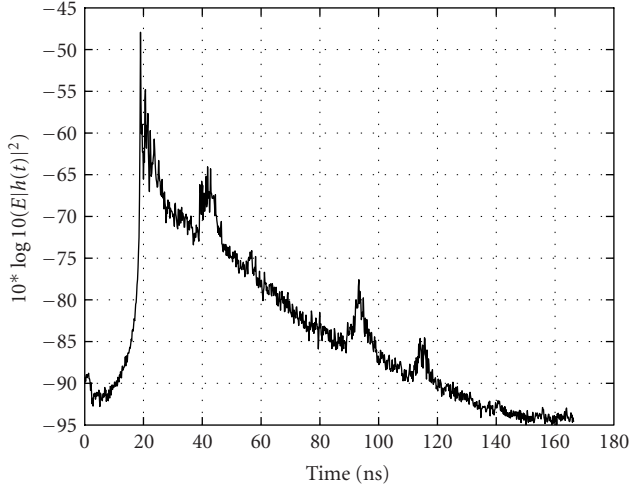
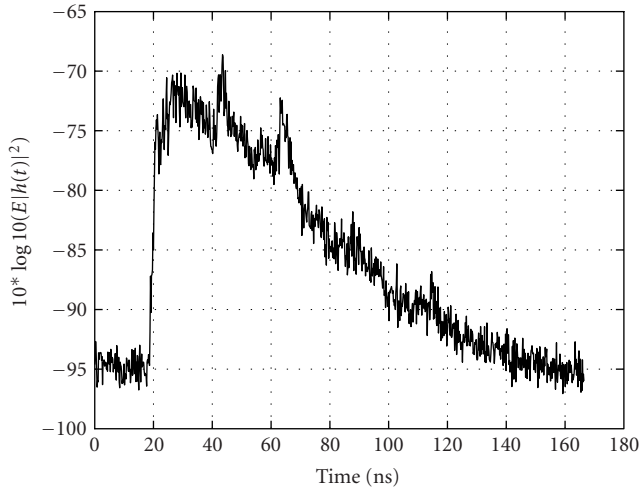FIGURE 6: Typical power intensity profile in LOS situation.

FIGURE 7: Typical power intensity profile in NLOS situation.

4.   EMPIRICAL MEASUREMENT RESULTS

4.1.   *Empirical distribution of eigenvalues*
for indoor UWB channels

The empirical results presented in this section are obtained from the LOS/NLOS 6 m scenarios described earlier. The sampled CIR is calculated from 6003 samples of the frequency response using IFFT, limited to 1000 samples for the computation of the sample covariance matrix, $\mathbf{K}_{\mathbf{h}}^{N}$. In Figures 6 and 7, we show the sample mean-power delay profile $(\operatorname{diag}(\mathbf{K}_{\mathbf{h}}^{N}))$ for the LOS and NLOS cases. We see that the LOS is characterized by two dominant clusters, one of which is around the LOS path, which is clearly visible. Secondary scatterers comprise significant energy nonetheless. In the NLOS case, there is dense scattering for short delays and the same secondary cluster as in the LOS scenario, resulting surely from multiple reflections in the room.
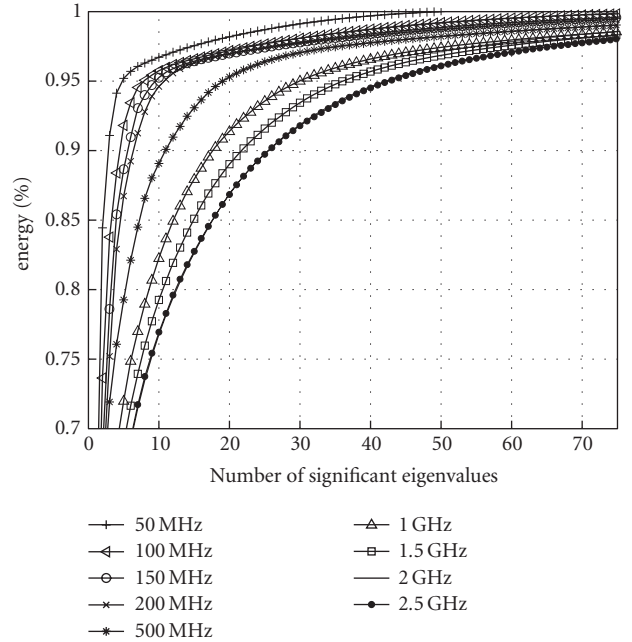

FIGURE 8: Fraction of the captured energy versus the number of significant eigenvalues in the LOS situation; resolution is 1 sample per MHz.
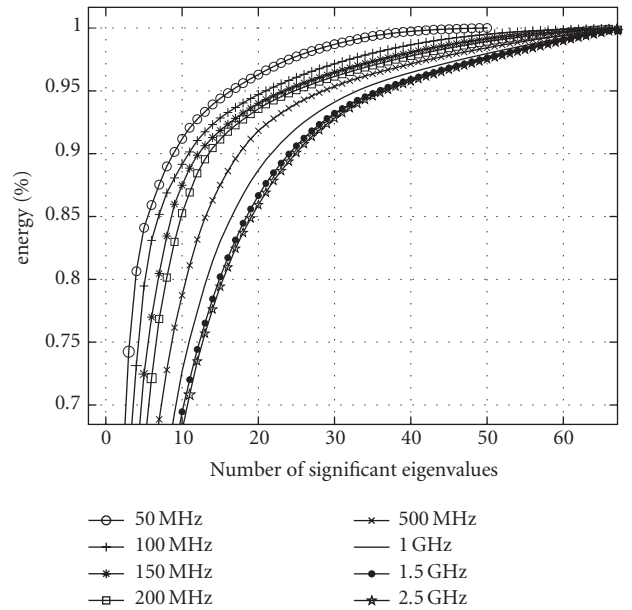

FIGURE 9: Fraction of the captured energy versus the number of significant eigenvalues in the NLOS situation.

In Figures 8 and 9, we plot, for the LOS and NLOS measurements, the fraction of the captured energy for M considered eigenvalues defined by $E_{M} = \sum_{i=1}^{M} \lambda_{i}(\mathbf{h}) / \sum_{i=1}^{N} \lambda_{i}(\mathbf{h})$, where N is the total number of eigenvalues. We remark in both plots, for the narrowband cases, that the majority of the channel energy (more than 90%) is confined in a small number of significant eigenvalues; whereas in the wide bandwidth
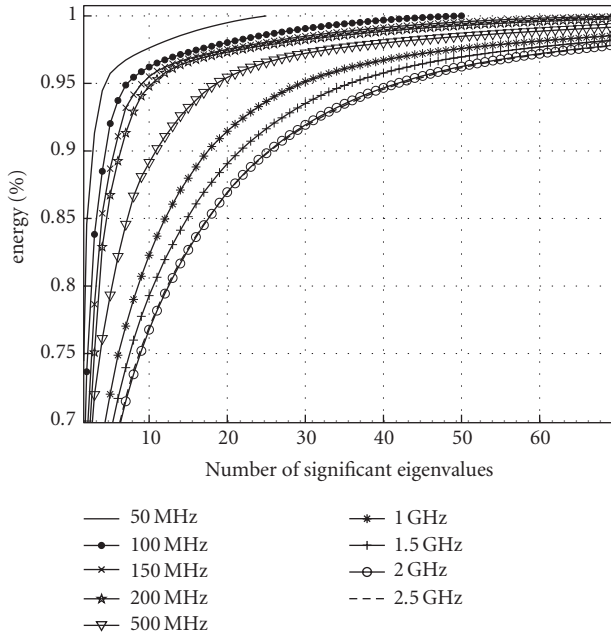
FIGURE 10: Fraction of the captured energy versus the number of significant eigenvalues in the LOS situation; resolution is 1 sample per 2 MHz.
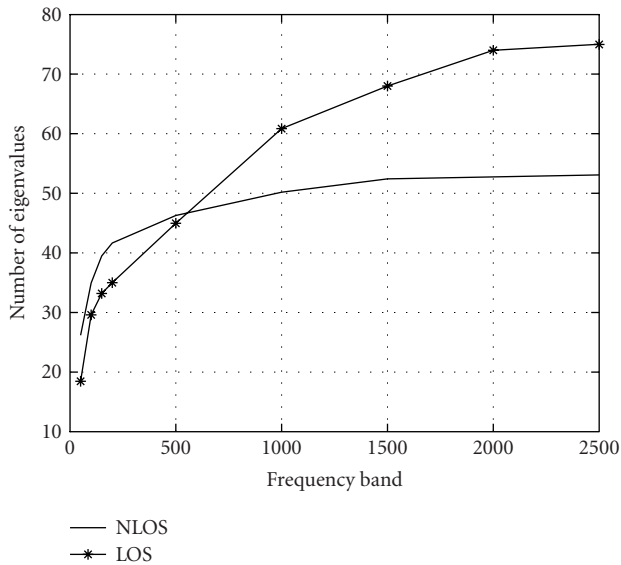

FIGURE 11: Evolution number of the eigenvalue for LOS and NLOS cases UWB measurement.

case, the channel energy is spread over a large number of eigenvalues (i.e., DoF). The results are obtained for a sampling rate, in the frequency domain, of 1 sample per MHz. This sampling resolution was verified to be sufficient to capture all channel DoFs and at the same time minimize the effect of time-domain aliasing as mentioned previously. Indeed, Figure 10 shows that increasing the sampling rate from 1 sample per 2 MHz to 1 sample per MHz does not modify channel eigenvalue distribution.
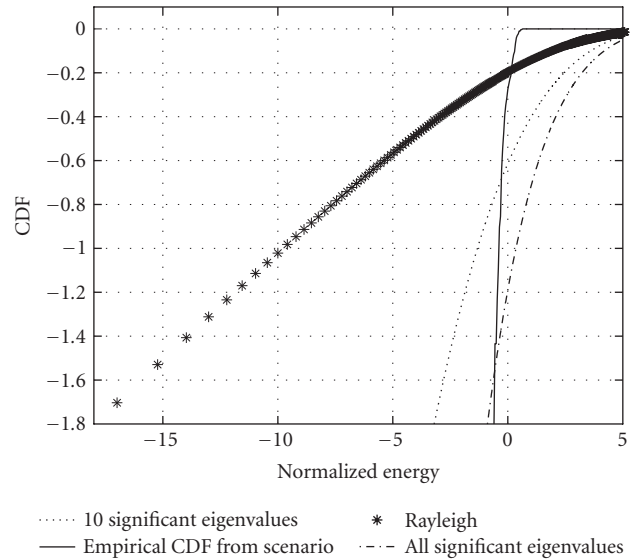

FIGURE 12: The empirical cumulative distribution function.

Figure 11, plotted for 98% captured energy, shows that the number of significant eigenvalues increases with the channel bandwidth, although not linearly. We see that in both cases, the increase is linear until approximately 200 MHz, where a saturation effect begins to occur. This means that until this critical bandwidth, the signal bandwidth does not provide sufficient resolution to resolve all eigenvalues, or equivalently the complete number of multipath components. Beyond this point, however, the channel is degenerate in the sense that all paths can be resolved. We note that the number of significant eigenvalues in the saturation region is markedly higher in the LOS case. This can be explained by the fact that the object placed between the transmitter and the receiver also shadows a significant portion of NLOS components, and the richness of the channel is therefore reduced.

The analysis of the empirical CDF of the normalized energy for the LOS case in Figure 12 shows that the CDF for a 6 GHz bandwidth exhibits a very sharp slope around the mean-signal strength (it is compared to a diversity of 1 Rayleigh channel to highlight the extreme behavior of these channels). We also compare the empirical CDF curve to that one obtained using the approximation in (12). We can see that the number of significant eigenvalues is directly related to the steepness of CDF curve. The high number of DoFs shows that UWB channels can be considered as deterministic (nonfading) in practice, provided receivers exploiting the full-channel energy are employed.

4.2. Eigenfunction analysis in LOS and NLOS situations

Figures 13, 14, and 15 show some sampled eigenfunctions in the LOS settings corresponding to the most significant eigenvalues. These figures show that the channel exhibits a clustered behavior, as can be seen when we plot the CIR shown
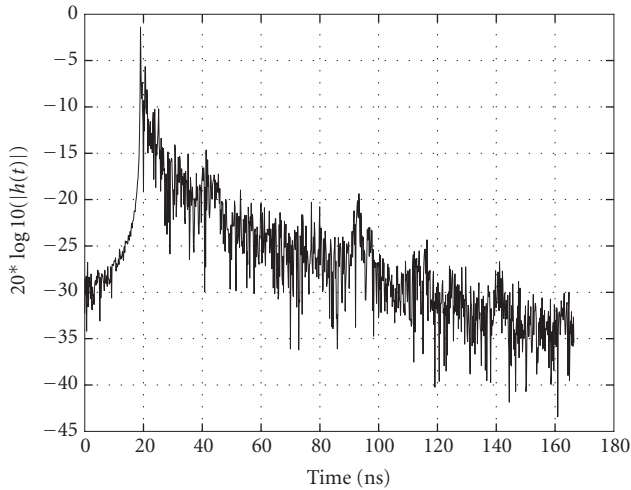
FIGURE 13: Eigenfunction corresponding to $\lambda_1 = 0.4445$ in the LOS situation.
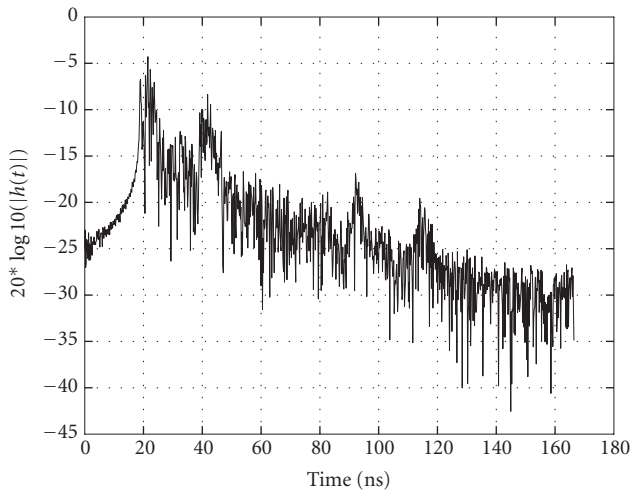

FIGURE 14: Eigenfunction corresponding to $\lambda_5 = 0.0314$ in the LOS situation.

in Figures 13 and 14. It is remarkable that from our analysis, we see that paths from different clusters have comparable strengths in the same eigenfunction. As a result, these clusters are strongly and statistically dependent as was described in the previous section.

5. CONCLUSION

In this work, we present results from UWB channel measurement campaigns conducted at Institut Eurécom Laboratories. These measurements confirm previous results performed in other laboratories (e.g., [3]) regarding the clustered behavior of the UWB channel as well as the multipath richness exposed by the extreme bandwidth. The new results published in this work are twofold; firstly, we show the evo-
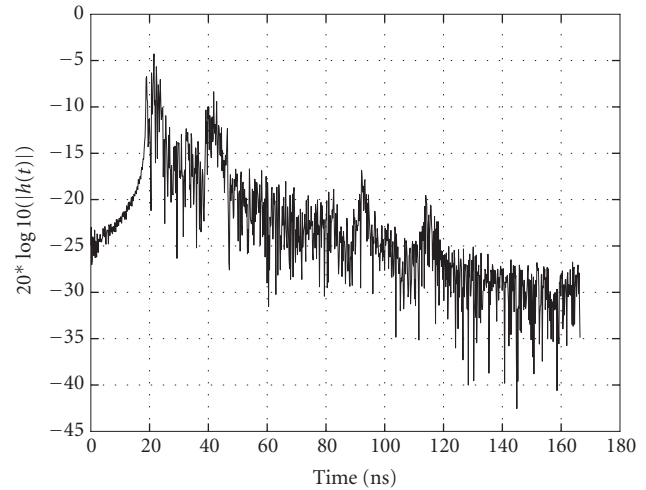

FIGURE 15: Eigenfunction corresponding to $\lambda_{10} = 0.0133$ in the LOS situation.

lution of the number of channel eigenvalues as a function of the system bandwidth for both LOS and NLOS scenarios, where we see that the number of eigenvalues tends to saturate for the extreme bandwidth of UWB systems. This seems to suggest that all significant multipath components can be resolved. Secondly, we show that there is a strong statistical dependence between paths coming from different clusters, which is assumed not to be the case in most propagation models.

REFERENCES

[1] R. A. Scholtz, "Multiple access with time-hopping impulse modulation," in *Proc. IEEE Military Communications Conference (MILCOM '93)*, vol. 2, pp. 447–450, Boston, Mass, USA, October 1993.

[2] M. Z. Win and R. A. Scholtz, "Impulse radio: how it works," *IEEE Commun. Lett.*, vol. 2, no. 2, pp. 36–38, 1998.

[3] J. Kunisch and J. Pamp, "Measurement results and modeling aspects for the UWB radio channel," in *Proc. IEEE Conference on Ultra Wideband Systems and Technologies (UWBST '02)*, pp. 19–23, Baltimore, Md, USA, May 2002.

[4] P. Pagani, P. Pajusco, and S. Voinot, "A study of the ultrawideband indoor channel: propagation experiment and measurement results," in *Proc. International Workshop on Ultra Wideband Systems (IWUWBS '03)*, Oulu, Finland, June 2003.

[5] J. Foerster, "Channel modeling sub-committee report final," IEEE P802.15- 02/490r0-SG3a, 2002.

[6] R. D. Wilson, R. D. Weaver, M.-H. Chung, and R. A. Scholtz, "Ultra wideband interference effects on an amateur radio receiver," in *Proc. IEEE Conference on Ultra Wideband Systems and Technologies (UWBST '02)*, pp. 315–319, Baltimore, Md, USA, May 2002.

[7] H. Hashemi, "Impulse response modeling of indoor radio propagation channels," *IEEE J. Select. Areas Commun.*, vol. 11, no. 7, pp. 967–978, 1993.

[8] H. Hashemi and D. Tholl, "Statistical modeling and simulation of the RMS delay spread of indoor radio propagation channels," *IEEE Trans. Veh. Technol.*, vol. 43, no. 1, pp. 110–120, 1994.

[9] H. Hashemi, "The indoor radio propagation channel," *Proc. IEEE*, vol. 81, no. 7, pp. 943–968, 1993.

[10] D.-S. Yoo, V. W.-K. Cheng, and W. E. Stark, "An index of frequency selectivity: frequency mean square correlation," in *IEEE 51st Vehicular Technology Conference (VTC '00)*, vol. 3, pp. 2546–2550, Tokyo, Japan, May 2000.

[11] P. A. Bello, "Characterization of randomly time-variant linear channels," *IEEE Trans. Communications*, vol. 11, no. 4, pp. 360–393, 1963.

[12] P. A. Bello, "Time-frequency duality," *IEEE Trans. Inform. Theory*, vol. 10, no. 1, pp. 18–33, 1964.

[13] G. Matz, A. F. Molisch, F. Hlawatsch, M. Steinbauer, and I. Gaspard, "On the systematic measurement errors of correlative mobile radio channel sounders," *IEEE Trans. Communications*, vol. 50, no. 5, pp. 808–821, 2002.

[14] D. Slepian and H. O. Pollak, "Prolate spheroidal wave functions, Fourier analysis and uncertainty. I," *Bell System Tech. J.*, vol. 40, pp. 43–64, 1961.

[15] M. Wax and T. Kailath, "Detection of signals by information theoretic criteria," *IEEE Trans. Acoustics, Speech, and Signal Processing*, vol. 33, no. 2, pp. 387–392, 1985.

[16] D. B. Williams, "Counting the degrees of freedom when using AIC and MDL to detect signals," *IEEE Trans. Signal Processing*, vol. 42, no. 11, pp. 3282–3284, 1994.

[17] T. W. Anderson, *An Introduction to Multivariate Statistical Analysis*, Wiley, New York, NY, USA, 2nd edition, 1984.

[18] T. Svantesson and J. Wallace, "Statistical characterization of the indoor MIMO channel based on LOS/NLOS measurements," in *Proc. 36th Asilomar Conference on Signals, Systems & Computers*, vol. 2, pp. 1354–1358, Pacific Grove, Calif, USA, November 2002.

[19] W. C. Jakes, *Microwave Mobile Communications*, John Wiley & Sons, New York, NY, USA, 1974.

[20] M. Schwartz, W. R. Bennett, and S. Stein, *Communication Systems and Techniques*, McGraw-Hill, New York, NY, USA, 1966.

[21] A. V. Oppenheim, A. S. Willsky, and I. T. Young, *Signals and Systems*, Prentice Hall, London, UK, 1983.

[22] D. A. Shnidman, "The calculation of the probability of detection and the generalized Marcum Q-function," *IEEE Trans. Inform. Theory*, vol. 35, no. 2, pp. 389–400, 1989.

[23] J. G. Proakis and D. G. Manolakis, *Digital Signal Processing: Principles, Algorithms and Applications*, Prentice Hall, Englewood Cliffs, NJ, USA, 3rd edition, 1996.

Aawatif Menouni Hayar received the Agrégation Génie Electrique degree from Ecole Normale Supérieure de Cachan, France, in 1992. She received the Diplôme d'Etudes Approfondies degree in signal processing image and communications and the degree of Engineering in communications systems and networks from ENSEEIHT de Toulouse, France, in 1997. She received the Ph.D. degree in signal processing and communications from Institut National Polytechnique de Toulouse, France, in 2001. She is currently a Research and Teaching Associate in Eurécom Mobile Communications Department, Sophia Antipolis, France. Her research interests include array of UWB channel measurements modeling and characterization, mobile and wireless communications (GSM, WCDMA, TD/CDMA), cross-layer design and radio resources management algorithms, and digital signal processing for software-defined radio.
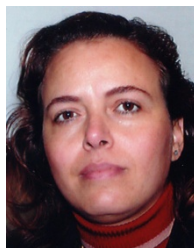
Raymond Knopp was born in Montreal, Canada, on January 20, 1969. He received the B.Eng. (honours) and M.Eng. degrees in electrical engineering from McGill University, Montreal, Canada, in 1992 and 1993, respectively. In 1997, he received the Ph.D. degree in communication systems from the Swiss Federal Institute of Technology (EPFL, http://www.epfl.ch), Lausanne. During his Ph.D. studies (1993–1997), he was a Research and Teaching Assistant in the Mobile Communications Department, Institut Eurécom, Sophia Antipolis, France. From 1997 to 2000, he was a Research Associate in the Mobile Communications Laboratory (LCM-EPFL), the Communication Systems Department, Swiss Federal Institute of Technology (EPFL), Lausanne. In 2000, he rejoined the Mobile Communications Department, Institut Eurécom, as an Associate Professor. His current research interests are in the area of digital communications, coding, multiple-access, ultra-wideband communications, sensor networks, software radio architectures, and implementation aspects of digital communication systems.

Rachid Saadane was born in El Jadida, Morocco, on January 10, 1979, He received his Bachelor's degree (License ès Sciences) in electronic physics and his Master's degree (DESA) in computer and telecommunication from the Faculty of Sciences, University Mohammed V, Rabat, Morocco, in 2003, and he developed his Master's Project at the Eurécom Institute, France. He is currently performing his Ph.D. degree in the University of Mohammed V, Rabat, Morocco, jointly with Eurécom Mobile Communications Department. His current research interests include UWB channel characterization, modeling, and wireless communication.